Biomolecules and Biomedicine
ISSN: 2831-0896 (Print) | ISSN: 2831-090X (Online)
Journal Impact Factor® (2024): 2.2
CiteScore® (2024): 5.2
www.biomolbiomed.com | blog.bjbms.org

RESEARCH ARTICLE

Xu et al: XY-01 hypochlorite imaging in cells

Hypochlorite sensing and real-time imaging with XY-01: A red-emitting fluorescent turn-on probe for living cells and colorectal cancer organoids

Yichun Xu[1,2#*], Zhihua Chen[3#], Jun Su[1,2#], Yanting Ding[1,2], Jiajing Zhou[2], Jiawei Zhao[2], Zhiyuan He[2], Yi Gong[2], Zhai Cai[4*], Lei Cui[3*], Junsong Han[2*]

[1]Department of Pathology, Shanghai Tongji Hospital, Tongji Hospital Affiliated to Tongji University, Shanghai, China;

[2]National Engineering Research Center for Biochip, Shanghai Biochip Limited Corporation, Shanghai, China;

[3]College of Science, Shanghai University, Shanghai, China;

[4]Department of General Surgery, Zhujiang Hospital, Southern Medical University, Guangzhou, China.

*Correspondence to Yichun Xu: crystalxyc@hotmail.com, Zhai Cai: czhaidr@126.com, Lei Cui: cuilei@shu.edu.cn, Junsong Han: junsong_han@shbiochip.com

[#]Equally contributed to this work: Yichun Xu, Zhihua Chen and Jun Su.

DOI: https://doi.org/10.17305/bb.2025.13312

ABSTRACT

Hypochlorite (ClO^-), a major reactive oxygen species generated in inflammation, is a potent biological oxidant involved in diverse physiological and pathological processes; therefore, sensitive detection of ClO^- is important for understanding disease pathophysiology and supporting early diagnosis and prevention. Here, we aimed to develop a physiologically compatible fluorescent tool for specific ClO^- sensing and imaging. We designed and synthesized a novel A–D–A type molecular fluorescent probe, XY-01, and characterized it by NMR, HRMS, UV–Vis and fluorescence spectroscopy. XY-01 operates through ClO^--triggered oxidation of a thioformyl group (C=S) to a carbonyl (C=O), which restores intramolecular charge transfer and produces a prominent fluorescence turn-on signal. In PBS (pH 7.4), XY-01 responded to ClO^- within 1 min with strong red emission at 666 nm and a large Stokes shift (~167 nm), showed high selectivity against common ions and reactive species, and achieved a detection limit of 3.39 μM within the biologically relevant range. Cytotoxicity assays indicated negligible toxicity, enabling real-time confocal imaging of ClO^- distribution in HCT-116 cells and colorectal cancer organoids. Collectively, XY-01 is a simple, sensitive, and low-toxicity probe that provides a promising platform for optical sensing and imaging of hypochlorite in living cells and organoids.

Keywords: Fluorescent probe, hypochlorite, organoid, cell imaging, near-infrared emission.

INTRODUCTION

The inflammation in biological systems is closely associated with the levels of reactive oxygen species (ROS) [1-2]. Hypochlorite (ClO^-) is one of the most crucial ROS and plays a complex role in various physiological and pathological processes [3]. It is generated by the catalysis of chloride ions and hydrogen peroxide (H_2O_2) by myeloperoxidase (MPO) [4-5]. Excessive ClO^- can oxidize key biomolecules, including proteins, nucleic acids, lipids, and enzymes, leading to significant tissue damage, inflammation, and the development of various diseases [6-10]. Elevated ClO^- levels exacerbate oxidative stress, which can compromise cell membranes, impair intercellular adhesion, and alter cellular viscosity [11]. These molecular alterations further amplify the immune response and disrupt normal cellular function, contributing to the progression of pathological conditions. Therefore, robust detection of ClO^- in living organisms is useful for understanding its roles in disease pathophysiology [12-13].

A variety of methods are available for detecting hypochlorite, including iodometric titration, colorimetry, chemiluminescence, coulometry, radiolysis [14-16]. However, these methods are often complex to implement and not be compatible with the physiological environment. Due to the high selectivity, rapid response, and low toxicity, fluorescent probes have been developed for a wide range of substrates. Fluorophores are essential in a wide range of scientific and technological applications, including bioimaging, diagnostics, and materials science [17-27]. Although some existing fluorescent probes demonstrated excellent performance including photostability, short response time, high sensitivity, and high selectivity, most of them used for ClO^- detection were poorly water-soluble, and not suitable for living cells [28]. However, the majority of the existing fluorescent probes required organic medium, which is not compatible with the aqueous physiological environment [29-30]. This limitation underscores the need for detection methods with enhanced sensitivity and selectivity, particularly those capable of operating effectively in aqueous environments and within the complex physiological conditions of living cells. Furthermore, detecting ClO^- within complex biological structures like living

organoids is more difficult, as these 3D models exhibit intricate interactions and diffusion properties that complicate detection. Despite these challenges, the continued development of advanced fluorescent probes holds great promise for enhancing our ability to monitor and understand ClO^--related processes in living organisms.

In this work, we synthesized a fast hypochlorite-responsive A-D-A type fluorescent probe (Scheme 1). The molecular structure of probe XY-01 was characterized by ^1H NMR, ^{13}C NMR, HRMS, UV-Vis, and fluorescence spectroscopy. The probe had a large Stokes shift (approximately 167 nm) and can respond to ClO^- within 1 min, with enhanced fluorescence intensity at 666 nm. The novel designed molecular fluorescent probe XY-01 could be used for optical sensing and imaging of hypochlorite within living cells and organoids, with the characteristic features of simple operation, low toxicity, high sensitivity, and high selectivity. Moreover, the fluorescent probe XY-01 demonstrated excellent performance of the adaptability with physiological conditions.

MATERIALS AND METHODS

Preparation of the fluorescence probe

The chemical reagents and solvents used in this study were purchased from commercial suppliers and used directly without further purification. ^1H NMR and ^{13}C NMR spectra were measured on a Bruker AV 500 spectrometer at room temperature. UV-visible absorption spectra were measured on a Techcomp UV2310II. PL spectra were recorded on a Hitachi F-4500. The fluorescence images of cells and organoids were obtained using confocal microscopy (Leica Stellaris5).

A possible mechanism of the designed probe was described in Scheme 1. The synthetic route of probe XY-01 was shown in Scheme 2. The compound 1 , 2 and 3 were prepared according to the literatures [31-32]. Structural identifications of XY-01 were confirmed by ^1H, ^{13}C NMR and HRMS spectrometry. The probe was dissolved in DMSO to prepare 10 mmol/L stock solution for later use. XY-01 featured a thioformyl group (-C=S) that acted as both the reactive moiety and the core unit disrupting ground-state ICT. ClO^- selectively oxidized this group to a carbonyl group

(-C=O). This oxidation enhanced the electron-withdrawing ability of the product, reconstructing the ICT pathway by reducing the electron transfer energy barrier from donor (D) to acceptor (A) units, thus recovering ICT. We explicitly correlated this ICT recovery with spectral changes: restored ICT induced a 167 nm redshift in absorption/emission spectra and eliminated thioformyl-induced fluorescence quenching, leading to prominent fluorescence enhancement (turn-on signal) (Scheme 3).

Cell culture

HCT-116 cells were purchased from the National Collection of Authenticated Cell Cultures (Shanghai, China). HCT-116 cells were cultured in RPMI-1640 medium supplemented with 10% (v/v) FBS. The cells were maintained in a humidified atmosphere of 5% CO_2 and 95% air at 37°C.

Analysis of probe toxicity on HCT-116 cells

HCT-116 cells were seeded at 1.0×105 cells/well in a 96-well plate and cultured overnight. Cells were treated with the probe at various concentrations (0, 10, 50, 100, 200 and 400μM) for 1h. After treatment, cell viability was evaluated with a CCK-8 assay following the manufacturer's instructions.

Confocal microscope imaging on HCT-116 cells

For further evaluation of probe XY-01 applied in imaging in cancer cells, HCT-116 cells were also chosen for cellular fluorescence imaging. HCT-116 cells were seeded at 1.0×10^5 cells/well in a 96-well plate and cultured overnight. Commercial 7.5% NaOCl/HOCl was diluted, titrated with standardized sodium thiosulfate using starch indicator, pH-adjusted to 7.4 with 10 mM PBS, and used within 24 h after dark storage at 4 °C to prevent degradation. There were four groups in this experiment, including the control group, the ClO^- addition group, the agonist group, and the antagonist group. In the control group, only 10μM probe XY-01 was added to coculture for 30 min. In the ClO^- addition group, the cells were treated with 1 mM NaOCl/HOCl for 30 min, and then were washed. Then, 10 μM probe XY-01 was added to coculture for 30 min. In the agonist group, HCT-116 cells were first

incubated with 1.0 μg/mL lipopolysaccharide (LPS) for 12 h, followed by incubation with 1.0 μg/mL phorbol 12-myristate 13-acetate (PMA) for 1 h. Then, 10 μM of probe XY-01 was added and co-incubated for 30 minutes. In the antagonist group, HCT-116 cells were first incubated with 200 μM 4-aminobenzoic acid hydrazide (ABAH) for 3 h, followed by incubation with 1.0 μg/mL LPS for 12 h. The cells were then incubated with 1.0 μg/mL PMA for 1 h, and then, incubated with 10 μM of probe XY-01 for 30 min. Finally, fluorescence imaging experiments for all the four groups were performed on a confocal microscope (Leica Stellaris5).

Generation and identification of patient-derived organoids (PDOs)

Colorectal tumor tissues were obtained from patients undergoing surgical resection at Zhujiang Hospital of Southern Medical University with written informed consent. Ethical approval was granted by the institutional ethics committee (Approval No. 2023-KY-165-01). Three PDO lines were established from surgically resected colorectal tumors according to the literature [33], and characterized by immunofluorescence staining of colorectal cancer markers, including caudal type homeobox 2 (CDX2), cytokeratin 20 (CK20), pan-cytokeratin (PAN-CK) and Ki-67 proliferation-associated nuclear antigen (Ki-67), to confirm their epithelial origin and cancer-specific features [34-35].

Analysis of probe toxicity on colorectal cancer organoids

Three lines of colorectal cancer organoids were used for evaluating the probe toxicity. Colorectal cancer organoids were first digested into single cells, and collected. Subsequently, single-cell suspension was dispensed into 96-well plate with approximately 3000 cells per well. After 10 min of solidification in the incubator at 37°C, 50 μL of the medium was added to each well. 48 h later, the medium that contained the probe XY-01(0, 10, 50, 100, 200 and 400μM) was replaced. After 2 h of probe XY-01 treatment, ATP values were examined using CellTiter-Glo 3D (G9683, Promega).

Confocal microscope imaging on colorectal cancer organoids

For further evaluation of probe XY-01 applied in imaging in PDOs, colorectal cancer

organoids were also chosen for cellular fluorescence imaging. Colorectal cancer organoids were first digested into single cells, and collected. Subsequently, single-cell suspension was dispensed into 96-well plate with approximately 3000 cells per well. After 10 min of solidification in the incubator at 37°C, 50 μL of the medium was added to each well. The preparation of 1 mM NaOCl/HOCl stock followed the method described previously. There were four groups in this experiment, including the control group, the ClO^- addition group, the agonist group, and the antagonist group. In the control group, only 10μM probe XY-01 was added to coculture with the organoids for 1 h. In the ClO^- addition group, the organoids were treated with 1 mM ClO^- (7.5% sodium hypochlorite aqueous solution) for 30 min, and then were washed. Then, 10 μM probe XY-01 was added to coculture with the organoids for 1 h. In the agonist group, the organoids were first incubated with 1.0 μg/mL LPS for 12 h, followed by incubation with 1.0 μg/mL PMA for 1 h. Then, 10 μM of probe XY-01 was added and co-incubated with the organoids for 30 minutes. In the antagonist group, the organoids were first incubated with 200 μM ABAH for 3 h, followed by incubation with 1.0 μg/mL LPS for 12 h. The organoids were then incubated with 1.0 μg/mL PMA for 1 h, and then, incubated with 10 μM of probe XY-01 for 1 h. Finally, fluorescence imaging experiments for all the four groups were performed on a confocal microscope (Leica Stellaris5).

Statistical analysis

Each experimental value was expressed as mean ±SD. Statistical analysis was performed using the software of GraphPad Prism 5.0 to evaluate the significance of differences between groups considered as $*P < 0.05$; $**P < 0.01$; $***P < 0.001$. All data represented the mean of triplicates.

RESULTS

Preparation of the fluorescence probe

The fluorescence probe XY-01 was prepared as the route shown in Scheme 2. The structural identifications of the probe were confirmed by ^1H, ^{13}C NMR and HRMS

spectrometry (Figure S1-4). HPLC analysis of XY-01 oxidation by ClO^- showed characteristic peaks for XY-01 (1.7 min) and its product XY-01-OH (6.2 min), with the latter peak increasing gradually upon ClO^- addition, which supports the mechanism that XY-01 reacts with ClO^- to form XY-01-OH (Figure S5).

Photophysical property

To investigate the effect of pH on the fluorescence response of the probe, the fluorescence intensities of XY-01 and the XY-01 + ClO^- system were measured in 10 mM PBS across a pH range of 3.0 to 8.0, as shown in Figure 1. As the pH increased, the fluorescence intensity (I_{666}) of the system gradually increased, which can be attributed to the deprotonation of the phenolic hydroxyl group of XY-01-OH under alkaline conditions. Therefore, the probe exhibited favorable condition for biological detection. A buffer solution with pH 7.4 was chosen for the following experiments.

The absorption spectra of XY-01 were shown in Figure 2, where XY-01 exhibited a peak at 342 nm. As shown in Figure 2A, XY-01 showed a red fluorescence emission peak at approximately 666 nm. The UV-visible absorption and fluorescence properties of the probe XY-01 in the presence of hypochlorite were investigated in PBS buffer (pH = 7.4, 1X). Upon addition of ClO^-, the absorption at 342 nm decreased, while a new absorption peak appeared at 499 nm and gradually intensified with increasing ClO^- concentration. This was attributed to the restoration of the intramolecular charge transfer (ICT) mechanism. XY-01 features a thioformyl group (-C=S) that acts as both the reactive moiety and the core unit disrupting ground-state ICT. As shown in Figures 2B, the reaction product of probe XY-01 with ClO^- had an excitation wavelength of 499 nm and an emission wavelength of 666 nm. The Stokes shift of XY-01 was calculated as the difference between the absorption maximum of its oxidized form (499 nm, consistent with the excitation wavelength λ_{ex}) and the emission maximum (666 nm), resulting in a value of 167 nm, which was relatively large among organic molecular probes. In PBS solution (pH = 7.4, 1X), the reaction product of probe XY-01 with hypochlorite existed in both deprotonated and protonated forms, but the emission at 666 nm corresponds to the deprotonated form.

Selectivity experiment

In general, fluorescent probes can be applied to target molecules for cellular im-aging. Due to the complex intracellular environment, which contains a variety of ROS and ions, it is critical to evaluate the selectivity of probe XY-01. To assess the specific recognition ability of the probe XY-01, fluorescence spectroscopy experiment was conducted. Various ions were added to the probe XY-01 solution, and incubated at room temperature for 90 minutes, followed by fluorescence spectral analysis. As shown in Figure 3, the fluorescence intensity at 666 nm did not show any significant change upon addition of other ROS or ions. However, when ClO^- was added, the fluorescence intensity increased significantly. These results indicated that probe XY-01 performed high selectivity and specificity toward ClO^- in cellular environments. Moreover, upon addition of ClO^-, the color of the solution changed from colorless to red, which was easily visible. This further verified that fluorescent probe XY-01 exhibited the capability of strong anti-interference and reacted specifically with ClO^- even in the presence of numerous interfering ions. In total, 13 different interfering analytes were tested, none of which significantly affected the ability of probe XY-01 to detect ClO^-.

Response time

Response time is not only an important factor to evaluate the performance of a probe, but also a key indicator for assessing whether the probe can adapt to detecting various environment. To determine the optimal response time, we monitored the fluorescence intensity changes of the XY-01 + ClO^- system at 666 nm. The response time of probe XY-01 to hypochlorite at different time points was measured at room temperature. The Figure 4A showed the fluorescence spectra of XY-01 at different time intervals (0-180 s) after addition of ClO^-. Upon the addition of ClO^- to the solution, the fluorescence intensity increased and reached equilibrium within 1 min. The fluorescence intensity reached its maximum at a wavelength of 666nm. The time-dependent fluorescence intensity changes of XY-01 upon addition of ClO^- with different concentration (0, 2 and 20 μM) was demonstrated in Figure 4B.

To further investigate the sensitivity of the probe, we conducted concentration

titration experiments for probe XY-01. Following the IUPAC-recommended formula: the limit of detection (LOD) = 3σ_blank/slope, the LOD of the probe was 3.39 μM, which was suitable for the physiological concentration range of hypochlorite (5-25 μM). Following the IUPAC-recommended formula: the limit of quantification (LOQ) = 10σ_blank/slope, the LOQ of the probe was 11.30 μM. The LOD and LOQ were determined using eight calibration points with three technical replicates performed for each concentration. These results indicated that probes XY-01 could rapidly and sensitively detect ClO^-. The fluorescence quantum yield (Φ) was determined using the relative method. Rhodamine 6G was used as the reference dye, and measurements were performed in PBS solution (pH = 7.4, 1X) under the same excitation conditions (499 nm) for both the probe and the reference. The fluorescence quantum yields (Φ) of XY-01 and XY-01-OH were 0.025 and 0.33, respectively.

Cytotoxic effect of the probe on HCT-116 cells

The cell viability after treatments of HCT-116 cells by the probe was evaluated by the CCK8 assay. The cytotoxicity of the probe against HCT-116 cells was shown in Figure 6. For 1h-treated HCT-116 cells, the cell viability for all the treated groups were all above 95% comparing to the control group. The result of the CCK8 assay showed that the probe exhibited negligible cytotoxicity toward HCT-116 cells (Figure 5). We also evaluated the cytotoxicity of the probe at 12 and 24 h; cell viability remained above 95 % at concentrations ≤ 200 μM, indicating its suitability for long-term live-cell imaging (Figure S6A and Figure S6B).

Fluorescence imaging of ClO^- in HCT-116 cells

Considering the low cytotoxicity of the probe XY-01, it was applied to detect intracellular ClO^- in HCT-116 cells. As shown in Figure 6A, HCT-116 cells incubated only with the probe XY-01 (10 μM) displayed ignorable fluorescence. In contrast, HCT-116 cells pretreated with ClO^- (1 mM) showed a remarkable fluorescence enhancement (Figure 6B). Fluorescence was markedly enhanced in the agonist group (Figure 6C), whereas it was scarcely detectable in the antagonist group (Figure 6D). These results demonstrated that the probe XY-01 could be used for detection of ClO^-

in living cells.

Cytotoxic effect of the probe XY-01 on colorectal cancer organoids

PDOs are generated from epithelial cells and reflect the characteristics of related tissues [36]. They are promising tools for drug screening and predicting patient response [37]. To further evaluate cytotoxic Effect of the probe XY-01, it was assessed in patient-derived colorectal cancer organoids, which recapitulate the heterogeneity and architecture of primary tumors. Three PDO lines were characterized by immunofluorescence staining of colorectal cancer markers, including CDX2, CK20, PAN-CK, and Ki-67. The result confirmed these PDO lines had their epithelial origin and cancer-specific features (Figure 7).

The cytotoxicity of the probe against three colorectal cancer organoids was shown in Figure 8. For 2h-treated colorectal cancer organoids, the cell viability for all the treated groups were all above 95% comparing to the control group. The result of the ATP assay showed that there was minimal cytotoxicity of the probe for colorectal cancer organoids (Figure 8). We also evaluated the cytotoxicity of the probe at 12 and 24 h; cell viability remained above 95 % at concentrations ≤ 400 μM, indicating its suitability for long-term live-organoid imaging (Figure S6C and Figure S6D).

Fluorescence imaging of ClO^- in colorectal cancer organoids

Considering the low cytotoxicity of the probe XY-01, it was applied to detect intracellular ClO^- in colorectal cancer organoids. As showed in Figure 9, colorectal cancer organoids incubated only with the probe XY-01 (10 μM) displayed ignorable fluorescence. In contrast, colorectal cancer organoids pretreated with ClO^- (1 mM) showed a remarkable fluorescence enhancement (Figure 9). Fluorescence in colorectal cancer organoids was markedly enhanced in the agonist group, whereas it was scarcely detectable in the antagonist group. These results demonstrated that the probe XY-01 could be used for detection of ClO^- in cancer organoids.

DISCUSSION

Hypochlorite (ClO^-) mediates complex physiological and pathological functions, and

its overproduction induces tissue damage, inflammation, and multiple diseases via oxidizing core biomolecules [1,38,39]. Despite the excellent photophysical properties of some reported fluorescent probes, the majority of these agents for ClO^- detection were limited by poor water solubility and thus cannot be applied in living cell.

In this work, we synthesized a fast hypochlorite-responsive A-D-A type fluorescent probe XY-01 for the highly selective and sensitive detection of ClO^- in biological systems. This probe relied on structure-responsive optical changes and exhibited a prominent fluorescence turn-on response toward ClO^-. The probe exhibited good selectivity toward ClO^- over the tested anions and ROS, though it should be noted that the influence of HOBr and $ONOO^-$ on the probe was not examined in the present study. Upon the addition of ClO^- to the solution, the probe exhibited a distinct response where the fluorescence intensity increased rapidly and reached equilibrium within 1 min.

With low cytotoxicity, the probe XY-01was applied in imaging ClO^- distribution in HCT-116 cells and colorectal cancer organoids in real time. Notably, these PDOs have demonstrated their capacity to accurately replicate tissue functions and structures in vivo, including the mimetic properties of organoids [40,41]. Specifically, the extent to which they replicate the physiological and pathological characteristics of native human tissues is crucial for ensuring their reliability and relevance in preclinical studies [42,43]. Therefore, the novel designed fluorescent probe XY-01 held the potential to detect the ClO^- levels in living organisms. The probe's inherent characteristics of long-term applicability and low cytotoxicity highlight its remarkable potential for live-cell and live-organoid imaging applications. Cytotoxicity assays at 12 h and 24 h demonstrated that cell viability remained above 95% at concentrations $\leq$ 200 μM for live-cell imaging and up to 400 μM for live-organoid imaging, confirming its favorable biocompatibility profile. Low-dose compatibility minimizes cellular perturbation in single-cell models, while high-dose tolerance ensures sufficient tissue penetration and stable signal acquisition in three-dimensional organoid systems. Notably, such properties enable the probe to bridge the gap between conventional cellular imaging and advanced organoid-based studies that

recapitulate *in vivo* microenvironments. Collectively, these traits lay a solid foundation for the probe's future utilization in long-term dynamic tracking of biological processes across cellular and organoid models.

However, limitations of the present study include the absence of evidence that the observed fluorescence originates from endogenously generated ClO^-, as neither HCT-116 cells nor PDOs were characterized for myeloperoxidase expression or activity. Additionally, the lack of whole-animal validation leaves the performance of the probe XY-01 in intact physiological or pathological environments untested. Longer-term photostability assays haven't be conducted in the present study to validate the performance of the probe.

CONCLUSION

In this study, we successfully designed and synthesized a novel A-D-A type fluorescent probe XY-01, for the highly selective and sensitive detection of ClO^- in biological systems. XY-01 featured a thioformyl group (-C=S) that acted as both the reactive moiety and the core unit disrupting ground-state ICT. The results demonstrated that probe XY-01 could rapidly respond to ClO^- within biologically relevant concentration ranges, with 666 nm fluorescence plateauing within 1 min, and it also had excellent selectivity and low detection limits. Mechanistically, XY-01 reacts with ClO^- to form XY-01-OH, enabling effective ClO^- quantification in biological matrices. Further investigations revealed that the probes XY-01 hold great potential for imaging ClO^- in living cells and organoids. Notably, under the experimental conditions used in this study, XY-01 also demonstrated adequate photostability to support endpoint imaging. In summary, we provided a novel designed molecular fluorescent probe for optical sensing and imaging of ClO^- within living cells and organoids, with the characteristic features of simple operation, low toxicity, appreciable sensitivity, high selectivity and the adaptability with physiological conditions, offering strong technical support for early disease diagnosis and prevention in the biomedical field.

Conflicts of interest: Authors declare no conflicts of interest.

Funding: This research was funded by the National Natural Science Foundation of China (Grant No. 82203232).

Data availability: Dataset available on request from the authors.

Submitted: October 2, 2025

Accepted: December 12, 2025

Published online: December 17, 2025

REFERENCES

1. Zhao M, Wang Y, Li L, Liu S, Wang C, Yuan Y, et al. Mitochondrial ROS promote mitochondrial dysfunction and inflammation in ischemic acute kidney injury by disrupting TFAM-mediated mtDNA maintenance. Theranostics. 2021;11(4):1845–63. https://doi.org/10.7150/thno.50905
2. Chen A, Huang H, Fang S, Hang Q. ROS: A "booster" for chronic inflammation and tumor metastasis. Biochim Biophys Acta Rev Cancer. 2024;1879(6):189175. https://doi.org/10.1016/j.bbcan.2024.189175
3. Sun M, Yu H, Zhu H, Ma F, Zhang S, Huang D, et al. Oxidative cleavage-based near-infrared fluorescent probe for hypochlorous acid detection and myeloperoxidase activity evaluation. Anal Chem. 2014;86(1):671–7. https://doi.org/10.1021/ac403603r
4. Lin W, Chen H, Chen X, Guo C. The roles of neutrophil-derived myeloperoxidase (MPO) in diseases: The new progress. Antioxidants (Basel). 2024;13(1):132. https://doi.org/10.3390/antiox13010132
5. Wu Y, Lun W, Zeng H, Guo X, Yang M, Lan Q. A facile near-infrared xanthene fluorescence probe for visualizing hypochlorous acid in vitro and in vivo. Analytica Chimica Acta. 2024;1294:342292. https://doi.org/10.1016/j.aca.2024.342292
6. Koide Y, Urano Y, Hanaoka K, Terai T, Nagano T. Development of an Si-rhodamine-based far-red to near-infrared fluorescence probe selective for hypochlorous acid and its applications for biological imaging. J Am Chem Soc. 2011;133(15):5680–2. https://doi.org/10.1021/ja111470n
7. Mehta NJ, Asmaro K, Hermiz DJ, Njus MM, Saleh AH, Beningo KA, et al. Hypochlorite converts cysteinyl-dopamine into a cytotoxic product: A possible

factor in Parkinson's disease. Free Radic Biol Med. 2016;101:44–52. https://doi.org/10.1016/j.freeradbiomed.2016.09.023

8. Chen S, Pan J, Gong Z, Wu M, Zhang X, Chen H, et al. Hypochlorous acid derived from microglial myeloperoxidase could mediate high-mobility group box 1 release from neurons to amplify brain damage in cerebral ischemia-reperfusion injury. J Neuroinflammation. 2024;21(1):70. https://doi.org/10.1186/s12974-023-02991-8
9. Shangguan L, Wang J, Qian X, Wu Y, Liu Y. Mitochondria-targeted ratiometric chemdosimeter to detect hypochlorite acid for monitoring the drug-damaged liver and kidney. Anal Chem. 2022;94(34):11881–8. https://doi.org/10.1021/acs.analchem.2c02431
10. Hou JT, Wang B, Zou Y, Fan P, Chang X, Cao X, et al. Molecular fluorescent probes for imaging and evaluation of hypochlorite fluctuations during diagnosis and therapy of osteoarthritis in cells and in a mouse model. ACS Sens. 2020;5(7):1949–58. https://doi.org/10.1021/acssensors.0c00270
11. Wang X, Song F, Peng X. A versatile fluorescent probe for imaging viscosity and hypochlorite in living cells. Dyes Pigments. 2016;125:89–94. https://doi.org/10.1016/j.dyepig.2015.10.012
12. Huang T, Yan S, Yu Y, Xue Y, Yu Y, Han C. Dual-responsive ratiometric fluorescent probe for hypochlorite and peroxynitrite detection and imaging in vitro and in vivo. Anal Chem. 2022;94(2):1415–24. https://doi.org/10.1021/acs.analchem.1c04729
13. Cheshchevik VT, Krylova NG, Cheshchevik NG, Lapshina EA, Semenkova GN, Zavodnik IB. Role of mitochondrial calcium in hypochlorite-induced oxidative damage of cells. Biochimie. 2021;184:104–15. https://doi.org/10.1016/j.biochi.2021.02.009
14. Mangum LC, Garcia GR, Niece KL, Wenke JC, Akers KS. A Rapid, High-Throughput Iodometric Titration Method for the Determination of Active

Chlorine Content of Topical Antiseptic Solutions. J Antimicrob Agents. 2017;3:152.

15. Gil D, Choi B, Lee JJ, Lee H, Kim KT, Kim C. A colorimetric/ratiometric chemosensor based on an aggregation-induced emission strategy for tracing hypochlorite in vitro and in vivo. Ecotoxicol Environ Saf. 2023;257:114954. https://doi.org/10.1016/j.ecoenv.2023.114954
16. Yin R, Ling L, Shang C. Wavelength-dependent chlorine photolysis and subsequent radical production using UV-LEDs as light sources. Water Res. 2018;142:452–8. https://doi.org/10.1016/j.watres.2018.06.018
17. Wang H, Yang J, Cao P, Guo N, Li Y, Zhao Y, et al. Functionalization of bismuth sulfide nanomaterials for their application in cancer theranostics. Chin Chem Lett. 2020;31(12):3015–26. https://doi.org/10.1016/j.cclet.2020.05.003
18. Liu S, Dong W, Gao HQ, Song Z, Cheng Z. Near-infrared-II fluorescent probes for analytical applications: From in vitro detection to in vivo imaging monitoring. Acc Chem Res. 2025;58(4):543–54. https://doi.org/10.1021/acs.accounts.4c00671
19. Liu Y, Yu Y, Zhao Q, Tang C, Zhang H, Qin Y, et al. Fluorescent probes based on nucleophilic aromatic substitution reactions for reactive sulfur and selenium species: Recent progress, applications, and design strategies. Coord Chem Rev. 2021;427:213601. https://doi.org/10.1016/j.ccr.2020.213601
20. Hricak H, Abdel-Wahab M, Atun R, Lette MM, Paez D, Brink JA, et al. Medical imaging and nuclear medicine: A Lancet Oncology Commission. Lancet Oncol. 2021;22(4):e136–e172. https://doi.org/10.1016/S1470-2045(20)30751-8
21. Rao J, Dragulescu-Andrasi A, Yao H. Fluorescence imaging in vivo: Recent advances. Curr Opin Biotechnol. 2007;18(1):17–25. https://doi.org/10.1016/j.copbio.2007.01.003

22. Schäferling M. The art of fluorescence imaging with chemical sensors. Angew Chem Int Ed Engl. 2012;51(15):3532–54. https://doi.org/10.1002/anie.201105459
23. Wu L, Sedgwick AC, Sun X, Bull SD, He XP, James TD. Reaction-based fluorescent probes for the detection and imaging of reactive oxygen, nitrogen, and sulfur species. Acc Chem Res. 2019;52(9):2582–97. https://doi.org/10.1021/acs.accounts.9b00302
24. Lv J, Chen Y, Wang F, Wei T, Zhang Z, Qiang J, et al. A mitochondria-targeted fluorescent probe based on fluorescein derivative for detection of hypochlorite in living cells. Dyes Pigments. 2018;148:353–8. https://doi.org/10.1016/j.dyepig.2017.09.037
25. Yamazaki T, Liu X, Chang YT, Arai S. Applicability and limitations of fluorescence intensity-based thermometry using a palette of organelle thermometers. Chemosensors. 2023;11(7):375. https://doi.org/10.3390/chemosensors11070375
26. Hori A, Matsumoto A, Ikenouchi J, Konishi GI. D-π-A fluorophores with strong solvatochromism for single-molecule ratiometric thermometers. J Am Chem Soc. 2025;147(11):9953–61. https://doi.org/10.1021/jacs.5c01173
27. Yang L, Hou H, Li J. Frontiers in fluorescence imaging: Tools for the in situ sensing of disease biomarkers. J Mater Chem B. 2025;13(4):1133–58. https://doi.org/10.1039/D4TB01867B
28. Song ZG, Yuan Q, Lv P, Chen K. Research progress of small molecule fluorescent probes for detecting hypochlorite. Sensors (Basel). 2021;21(19):6326. https://doi.org/10.3390/s21196326
29. Liu Q, Liu C, He S, Zhao L, Zeng X, Zhou J, et al. A new phenylazo-based fluorescent probe for sensitive detection of hypochlorous acid in aqueous solution. Molecules. 2022;27(9):2978. https://doi.org/10.3390/molecules27092978

30. Zhang J, Yang M, Mazi W, Adhikari K, Fang M, Xie F, et al. Unusual fluorescent responses of morpholine-functionalized fluorescent probes to pH via manipulation of BODIPY's HOMO and LUMO energy orbitals for intracellular pH detection. ACS Sens. 2016;1(2):158–65. https://doi.org/10.1021/acssensors.5b00065
31. Kopp F, Krasovskiy A, Knochel P. Convenient magnesiation of aromatic and heterocyclic rings bearing a hydroxy group in presence of LiCl. Chem Commun. 2004;(20):2288–9. https://doi.org/10.1039/b409664a
32. Hoegl H. On photoelectric effects in polymers and their sensitization by dopants. J Phys Chem. 1965;69(3):755–66. https://doi.org/10.1021/j100887a008
33. Jung P, Sato T, Merlos-Suárez A, Barriga FM, Iglesias M, Rossell D, et al. Isolation and in vitro expansion of human colonic stem cells. Nat Med. 2011;17(10):1225–7. https://doi.org/10.1038/nm.2470
34. Furbo S, Urbano PCM, Raskov HH, Troelsen JT, Fiehn AMK, Gögenur I. Use of patient-derived organoids as a treatment selection model for colorectal cancer: A narrative review. Cancers (Basel). 2022;14(4):1069. https://doi.org/10.3390/cancers14041069
35. Tang DW, Chen IC, Chou PY, Lai MJ, Liu ZY, Tsai KK, et al. HSP90/LSD1 dual inhibitors against prostate cancer as well as patient-derived colorectal organoids. Eur J Med Chem. 2024;278:116801. https://doi.org/10.1016/j.ejmech.2024.116801
36. Atanasova VS, Cardona CDJ, Hejret V, Tiefenbacher A, Mair T, Tran L, et al. Mimicking tumor cell heterogeneity of colorectal cancer in a patient-derived organoid-fibroblast model. Cell Mol Gastroenterol Hepatol. 2023;15(6):1391–1419. https://doi.org/10.1016/j.jcmgh.2023.02.014

37. Verduin M, Hoeben A, De Ruysscher D, Vooijs M. Patient-derived cancer organoids as predictors of treatment response. Front Oncol. 2021;11:641980. https://doi.org/10.3389/fonc.2021.641980

FIGURES WITH LEGENDS

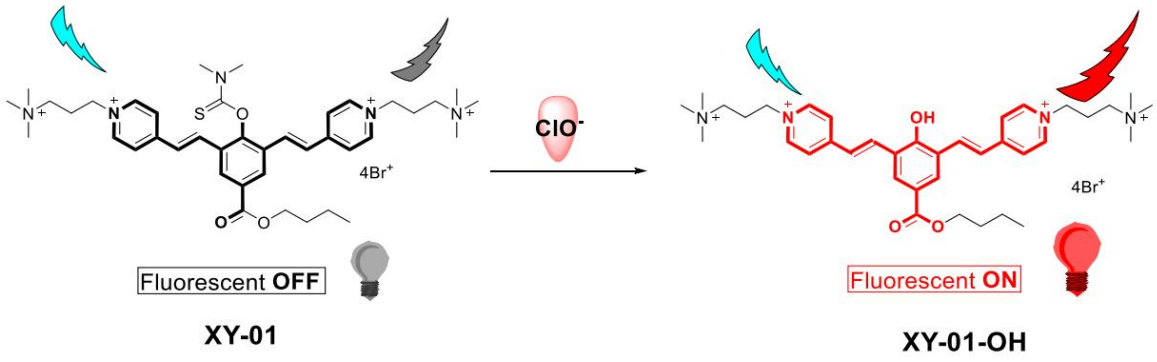

Scheme 1. Proposed reaction mechanism of probe XY-01 with ClO^-. The interaction of XY-01 with ClO^- results in the formation of the oxidized product XY-01-OH, thereby transitioning the probe from a fluorescence OFF state to a fluorescence ON state.

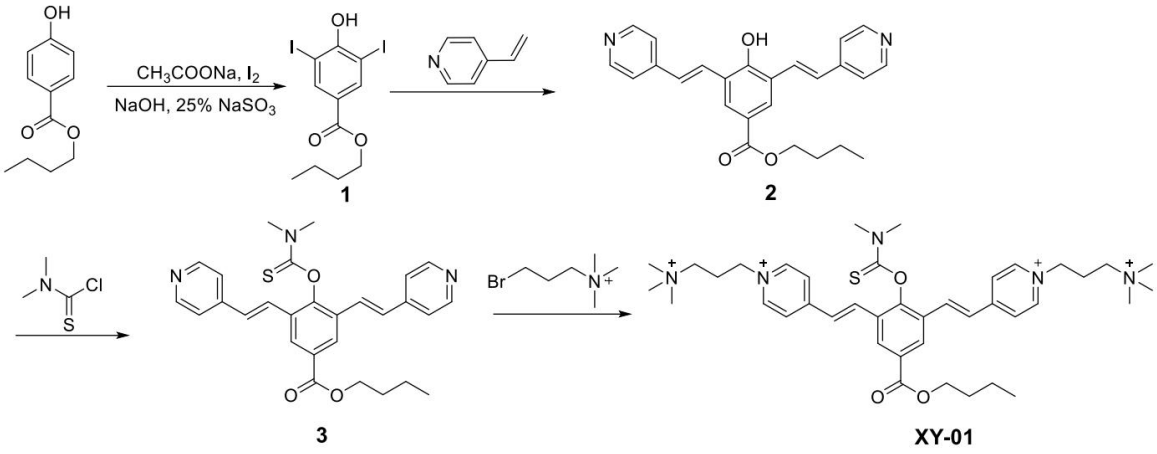

Scheme 2. Synthesis route of probe XY-01. The synthesis of XY-01 is illustrated through intermediates 1–3, which were produced following established protocols in the literature [31–32]. The structure of the final probe, XY-01, was validated using ^1H NMR, ^{13}C NMR, and high-resolution mass spectrometry (HRMS).

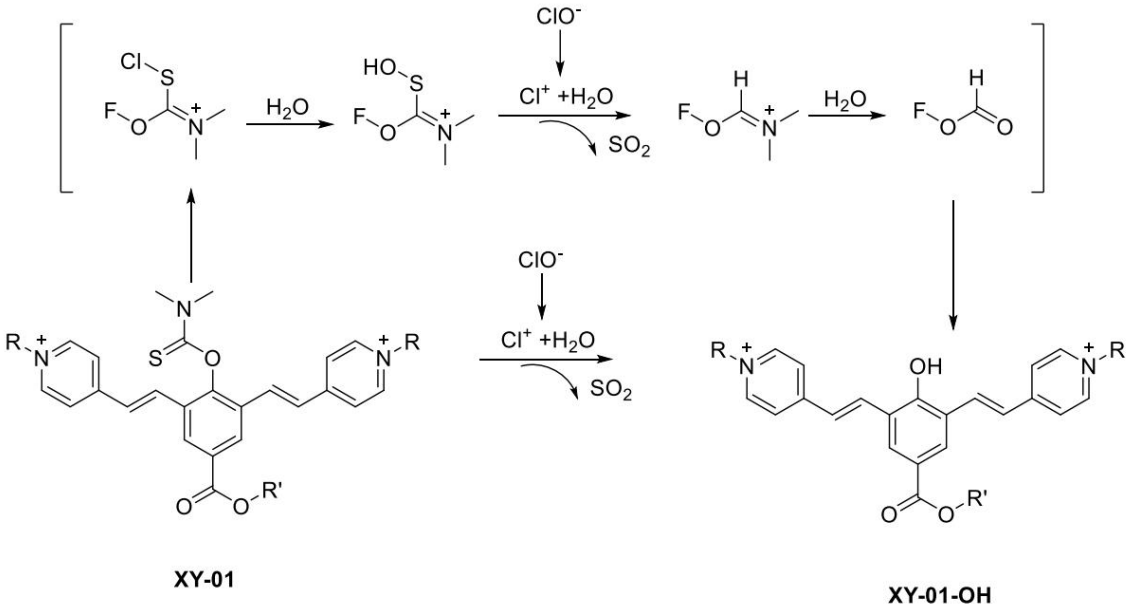

Scheme 3. Reaction mechanism of probe XY-01. The chloride ion (ClO^-) oxidizes the thioformyl group in XY-01, yielding the corresponding carbonyl product (XY-01-OH). This reaction restores intramolecular charge transfer (ICT) and generates a fluorescence turn-on response, accompanied by an approximately 167 nm redshift in both absorption and emission.

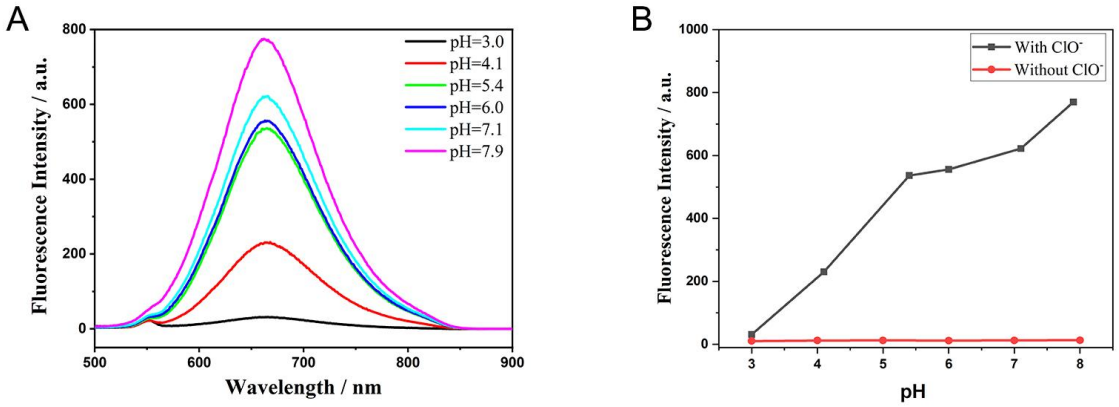

Figure 1. pH-dependent fluorescence response of XY-01 toward hypochlorite in 10 mM PBS. (A) Fluorescence emission spectra of XY-01 (10.0 μM) in the presence of ClO^- (1.0 mM) recorded at different pH values (3.0–7.9). (B) Fluorescence intensity at 666 nm (I_{666}) of XY-01 alone and XY-01 + ClO^- as a function of pH (3.0–8.0), showing a gradual increase in signal at higher pH attributed to deprotonation of the phenolic hydroxyl group of XY-01-OH. Abbreviations: PBS: Phosphate-buffered saline; ClO^-: Hypochlorite; I_{666}: Fluorescence intensity at 666 nm.

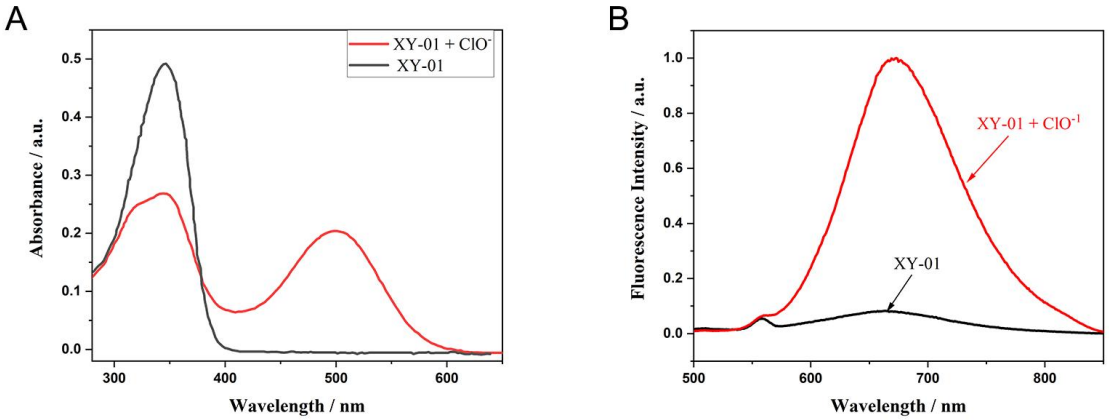

Figure 2. UV–Vis and fluorescence response of XY-01 to hypochlorite in PBS (pH 7.4, 1×). (A) Absorption spectra of XY-01 (10.0 μM) before (black) and after addition of ClO^- (1.0 mM, red), showing attenuation of the 342 nm band and appearance of a new absorption band at 499 nm (consistent with ICT restoration). (B) Fluorescence emission spectra of XY-01 (10.0 μM) without (black) and with ClO^- (1.0 mM, red) recorded at λ_{ex} = 499 nm (slit 5/5 nm), giving a strong turn-on emission

at ~666 nm (Stokes shift ~167 nm). Abbreviations: PBS: Phosphate-buffered saline; ClO^-: Hypochlorite; UV–Vis: Ultraviolet–visible; ICT: Intramolecular charge transfer.

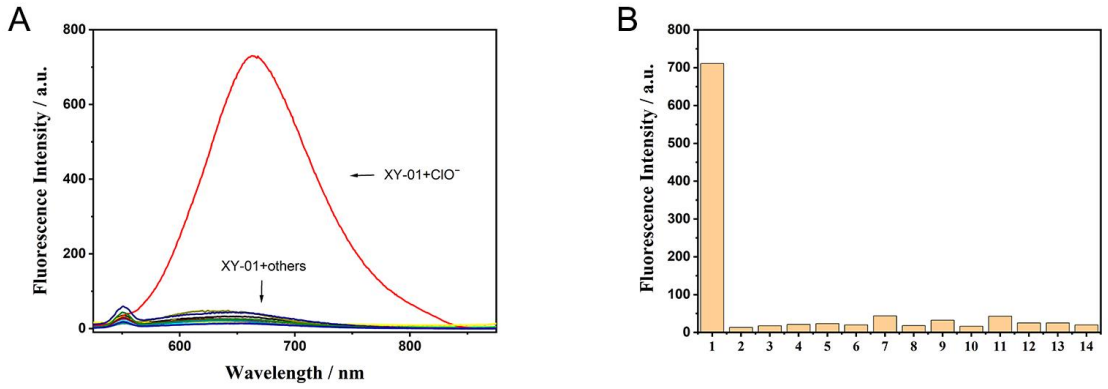

Figure 3. Selectivity of probe XY-01 toward hypochlorite. (A) Fluorescence emission spectra of XY-01 (10.0 μM) after incubation with ClO^- or other tested ions/ROS (each 1.0 mM) for 90 min at room temperature (λ_{ex} = 499 nm), showing a pronounced turn-on signal only in the presence of ClO^- ($\lambda_{em} \approx$ 666 nm). (B) Corresponding fluorescence intensities at 666 nm for XY-01 with different analytes (1–14): ClO^-, $S_2O_3^{2-}$, SO_4^{2-}, Br^-, Cl^-, Mg^{2+}, SO_3^{2-}, HSO_3^-, Cu^{2+}, CH_3COO^-, CO_3^{2-}, K^+, OH^-, H_2O_2. Abbreviations: ClO^-: Hypochlorite; ROS: Reactive oxygen species; λ_{ex}: Excitation wavelength; λ_{em}: Emission wavelength.

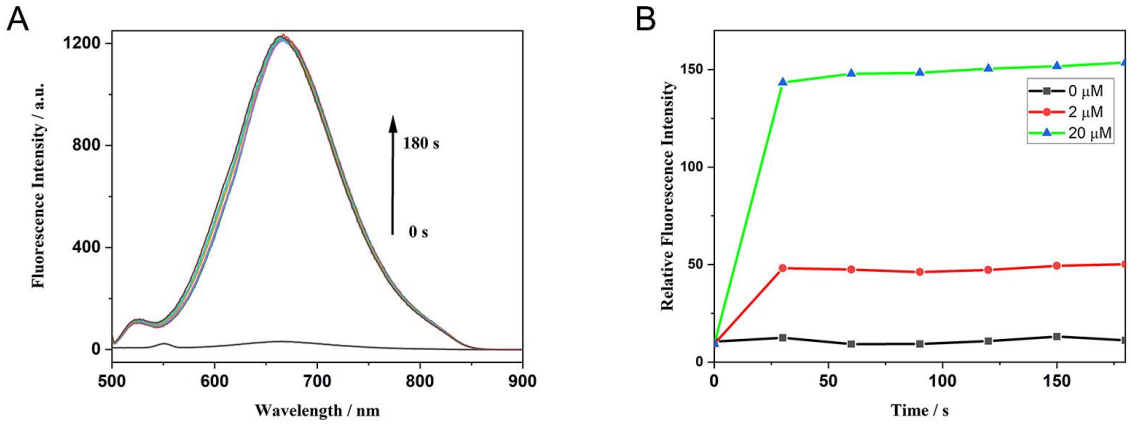

Figure 4. Response kinetics of XY-01 toward hypochlorite. (A) Time-resolved fluorescence emission spectra of XY-01 recorded from 0 to 180 s after addition of ClO^-, showing a rapid signal increase with the emission maximum at 666 nm and

equilibration within ~1 min. (B) Time-dependent fluorescence intensity changes of XY-01 upon treatment with different ClO^- concentrations (0, 2, and 20 μM).

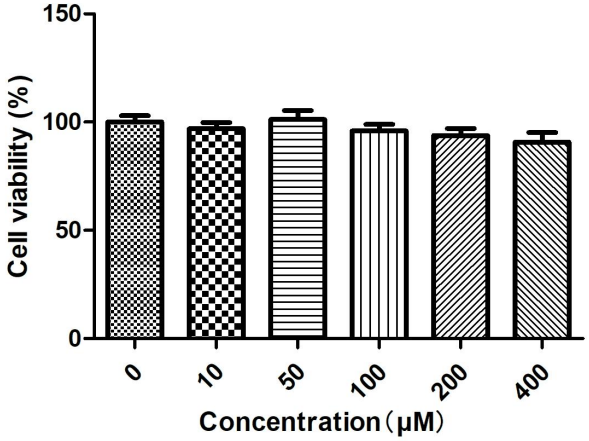

Figure 5. Cytotoxicity evaluation of XY-01 in HCT-116 cells. Cell viability after 1 h incubation with increasing concentrations of XY-01, determined by the CCK-8 assay; all treated groups maintained >95% viability relative to the untreated control. Abbreviations: CCK-8: Cell Counting Kit-8; HCT-116: human colorectal carcinoma cell line.

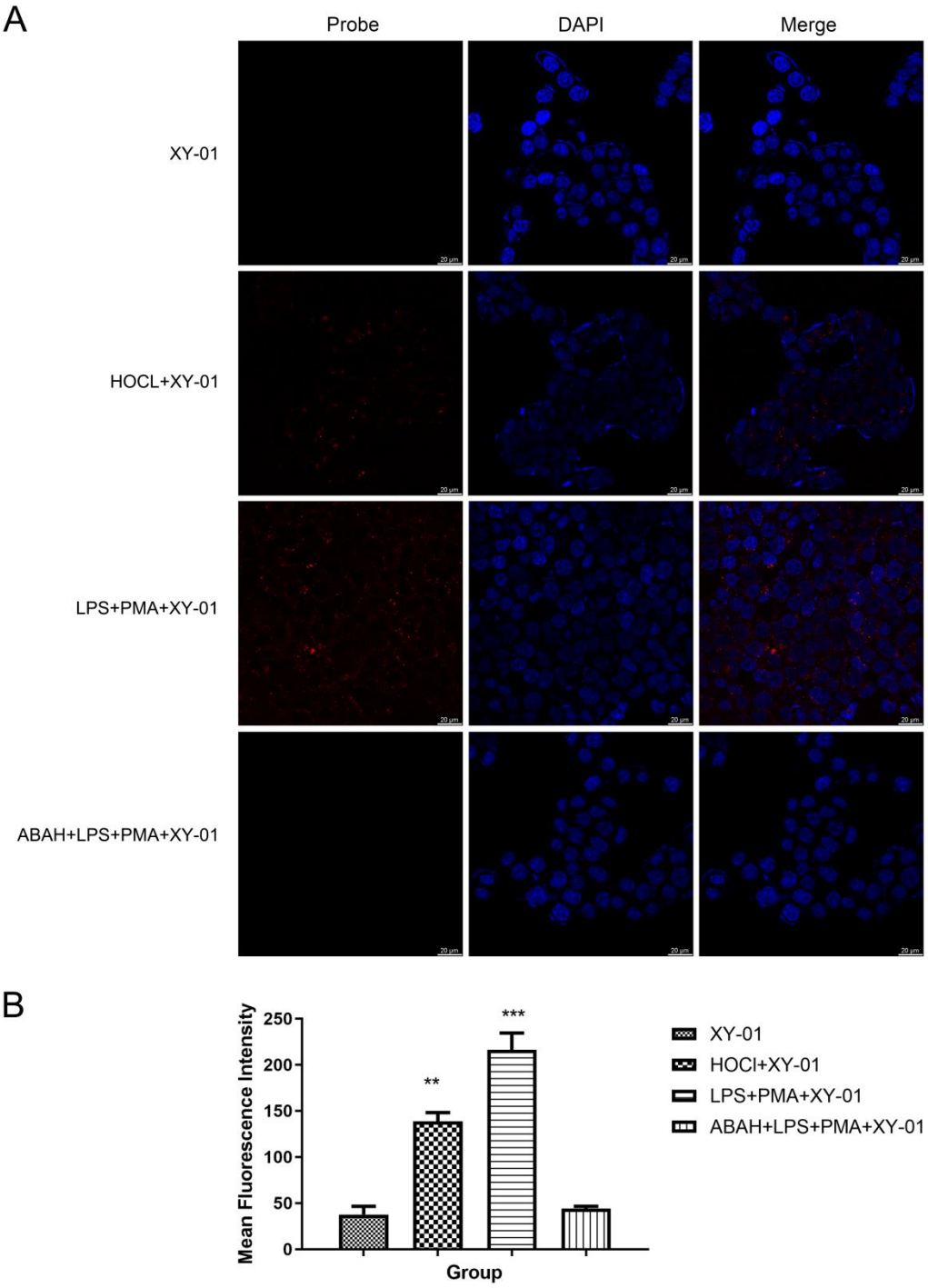

Figure 6. Confocal fluorescence imaging of intracellular hypochlorite in HCT-116 cells using probe XY-01. (A) Representative confocal images showing the XY-01 channel (Probe), nuclear staining (DAPI), and merged images for four conditions: cells incubated with XY-01 alone (10 μM, 30 min), cells pretreated with HOCl (1 mM, 30 min) followed by XY-01 staining, agonist-stimulated cells (LPS, 1.0 μg/mL,

12 h; then PMA, 1.0 μg/mL, 1 h) followed by XY-01 staining, and antagonist-treated cells (ABAH, 200 μM, 3 h) prior to LPS/PMA stimulation and XY-01 staining. Scale bar: 20 μm. Imaging settings: laser lines 405 nm/465 nm; detector HyD S1/HyD S2; pinhole 77.2 μm; gain 6.8/2.5; dwell time 1.575 μs. (B) Quantification of mean fluorescence intensity for each group (*P < 0.05, **P < 0.01, ***P < 0.001). Abbreviations: ABAH: 4-aminobenzoic acid hydrazide; DAPI: 4′,6-diamidino-2-phenylindole; HCT-116: human colorectal carcinoma cell line; HOCl: hypochlorous acid; HyD: hybrid detector; LPS: lipopolysaccharide; PMA: phorbol 12-myristate 13-acetate.

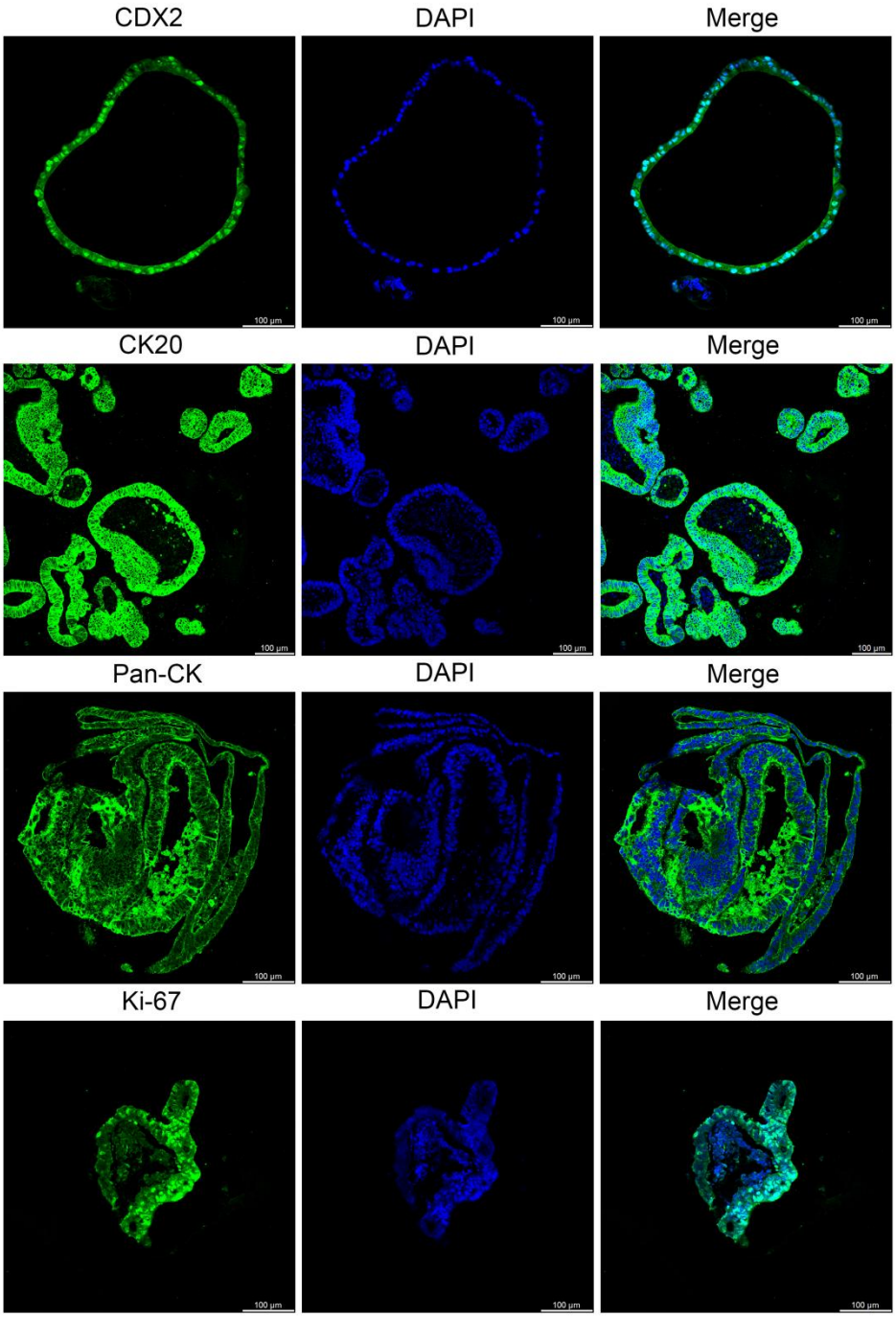

Figure 7. Confocal microscopy images for the identification of colorectal cancer organoids. Antibodies targeting CDX2 (intestinal epithelial cell marker), CK20 (intestinal epithelial cell marker), PAN-CK (epithelial cell marker), and Ki-67 (cell proliferation marker) were utilized. DAPI was employed to stain the nuclei. Scale bar: 100 μm; Laser wavelengths: 405 nm/488 nm; Detectors: HyD S1/HyD S2; Pinhole diameter: 53.1 μm; Gain settings: 21.4/2.5; Dwell time: 1.575 μs. Abbreviations:

CDX2: Caudal type homeobox 2; CK20: Cytokeratin 20; PAN-CK: Pan-cytokeratin; Ki-67: Ki-67 proliferation-associated nuclear antigen; DAPI: 4′,6-diamidino-2-phenylindole; HyD: Hybrid detector.

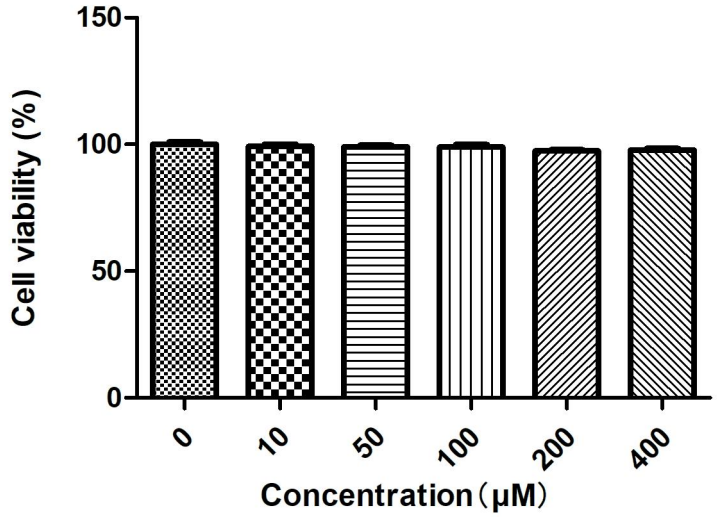

Figure 8. Cytotoxicity assessment of XY-01 in colorectal cancer organoids. Organoid viability after 2 h exposure to increasing concentrations of XY-01, measured by an ATP-based assay; all treated groups maintained >95% viability relative to the untreated control, indicating minimal cytotoxicity under the experimental conditions.

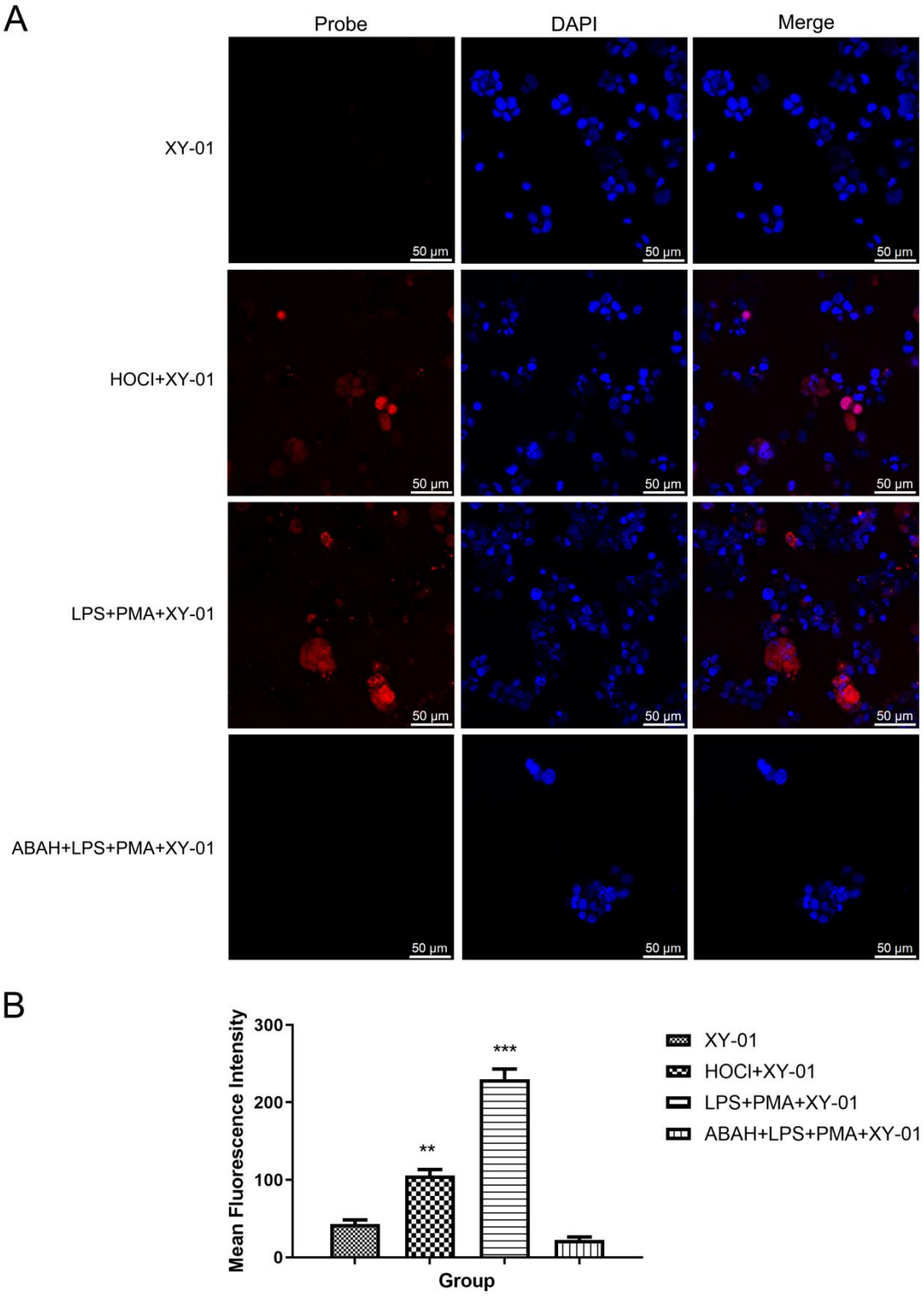

Figure 9. Confocal fluorescence imaging of intracellular hypochlorite in colorectal cancer organoids using probe XY-01. (A) Representative confocal images showing the XY-01 channel (Probe), nuclear staining (DAPI), and merged images under four conditions: organoids incubated with XY-01 alone (10 μM;

negligible fluorescence), organoids pretreated with HOCl (1 mM) followed by XY-01 staining (enhanced fluorescence), agonist-stimulated organoids (LPS + PMA) followed by XY-01 staining (marked fluorescence increase), and antagonist-treated organoids (ABAH + LPS + PMA) followed by XY-01 staining (fluorescence strongly suppressed). Scale bar: 50 μm. Imaging settings: laser lines 405 nm/465 nm; detector HyD S1/HyD S2; pinhole 77.2 μm; gain 10.9/2.5; dwell time 1.575 μs. (B) Quantification of mean fluorescence intensity for each group (*P < 0.05, **P < 0.01, ***P < 0.001). Abbreviations: ABAH: 4-aminobenzoic acid hydrazide; DAPI: 4′,6-diamidino-2-phenylindole; HyD: hybrid detector; LPS: lipopolysaccharide; PMA: phorbol 12-myristate 13-acetate.

SUPPLEMENTAL DATA

Supplemental data are available at the following link:

https://www.bjbms.org/ojs/index.php/bjbms/article/view/13312/4083